



OPEN ACCESS

EDITED BY
Adolfo Poma,
Institute of Fundamental Technological
Research, Polish Academy of Sciences,
Poland

REVIEWED BY
Adam Liwo,
University of Gdansk, Poland
Thu Tran,
Vietnam National University, Vietnam

*CORRESPONDENCE
Mateusz Chwastyk,
✉ chwastyk@ifpan.edu.pl

†Deceased

SPECIALTY SECTION
This article was submitted to Recent
Advances in Computational Modelling of
Biomolecular Complexes,
a section of the journal
Frontiers in Chemistry

RECEIVED 23 November 2022
ACCEPTED 29 December 2022
PUBLISHED 25 January 2023

CITATION
Pham DQH, Chwastyk M and Cieplak M
(2023), The coexistence region in the Van
der Waals fluid and the liquid-liquid
phase transitions.
Front. Chem. 10:1106599.
doi: 10.3389/fchem.2022.1106599

COPYRIGHT
© 2023 Pham, Chwastyk and Cieplak. This
is an open-access article distributed under
the terms of the [Creative Commons
Attribution License \(CC BY\)](https://creativecommons.org/licenses/by/4.0/). The use,
distribution or reproduction in other
forums is permitted, provided the original
author(s) and the copyright owner(s) are
credited and that the original publication in
this journal is cited, in accordance with
accepted academic practice. No use,
distribution or reproduction is permitted
which does not comply with these terms.

The coexistence region in the Van der Waals fluid and the liquid-liquid phase transitions

Dinh Quoc Huy Pham, Mateusz Chwastyk* and Marek Cieplak†

Institute of Physics, Polish Academy of Sciences, Warsaw, Poland

Cellular membraneless organelles are thought to be droplets formed within the two-phase region corresponding to proteinaceous systems endowed with the liquid-liquid transition. However, their metastability requires an additional constraint—they arise in a certain region of density and temperature between the spinodal and binodal lines. Here, we consider the well-studied van der Waals fluid as a test model to work out criteria to determine the location of the spinodal line for situations in which the equation of state is not known. Our molecular dynamics studies indicate that this task can be accomplished by considering the specific heat, the surface tension and characteristics of the molecular clusters, such as the number of component chains and radius of gyration.

KEYWORDS

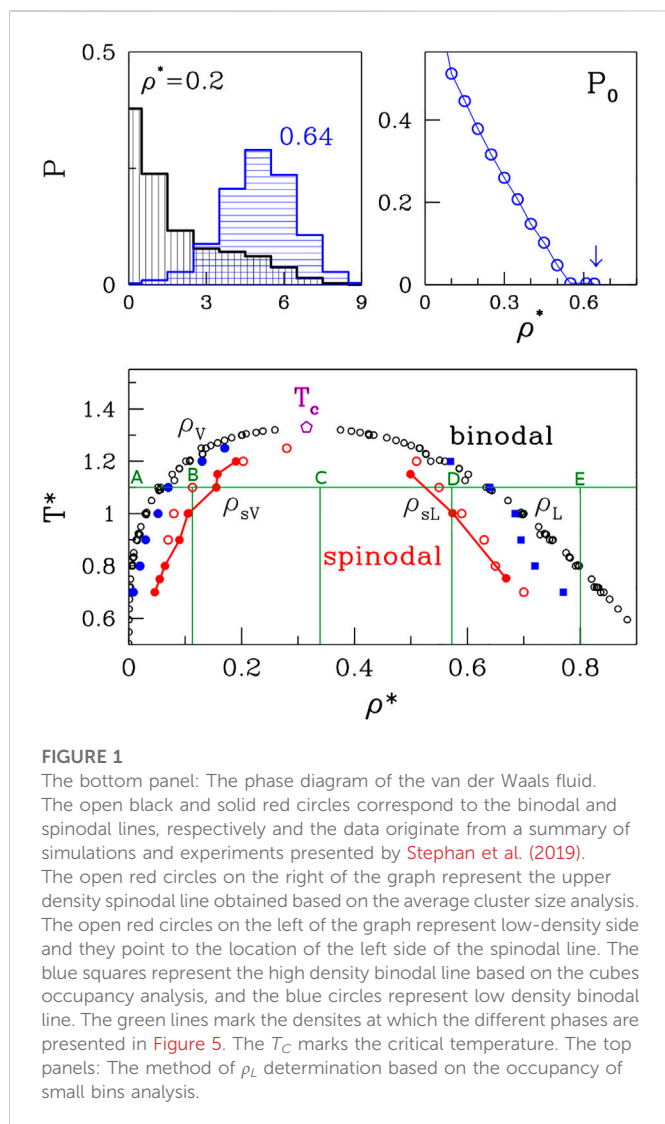
Van der Waals fluid, phase diagram, liquid-liquid phase transitions, intrinsically disordered proteins (IDPs), molecular dynamics simulations (MD)

1 Introduction

Cellular organelles can be either membraneless or membrane-bound. The membranes arise as droplets during a liquid-liquid phase transition (Brangwynne et al., 2009; Brangwynne et al., 2011; Shin and Brangwynne, 2017; Boeynaems et al., 2018; Elbaum-Garfinkle, 2019) as a result of thermal fluctuations. These biological droplets can be micrometers in size and exhibit hydrodynamical characteristics such as fusion (Caragine et al., 2018; Caragine and Haley, 2019). Proteinaceous liquids involved in the phase transition have been found to be composed primarily of intrinsically disordered proteins (IDPs) (Uversky, 2002; Dyson and Wright, 2005; Fink, 2005; Dunker et al., 2008; Ferreon et al., 2010; Uversky and Dunker, 2010; Babu et al., 2011; Wright and Dyson, 2015; Banani et al., 2017; Chwastyk and Cieplak, 2020; de Aquino et al., 2020) that allow for a multitude of ways to bind and aggregate.

The droplets may form only within the coexistence region of the phase diagram of the two fluids but their functionality requires that they are metastable. The paradigm model that yields such a coexistence region is the van der Waals (vdW) fluid as described by the well-known equation of state that generalizes the perfect gas law. In the density (ρ)—temperature (T) plane, the phase diagram of the vdW fluid includes the coexistence region of gas and liquid that is bounded by the inverted parabola, as shown in the bottom panel of Figure 1. Its vertex corresponds to the critical temperature (T_c) above which one cannot distinguish between the two phases. Such a phase diagram can be obtained for the system of n_m monatomic particles that interact through the 6–12 Lennard-Jones (LJ) potential (Hensen and McDonald, 1973) given by:

$$\Phi_{LJ} = 4\epsilon \left[\left(\frac{\sigma}{r} \right)^{12} - \left(\frac{\sigma}{r} \right)^6 \right], \quad (1)$$



where ε and σ are the uniform energy and length parameters. A significant increase in ρ , at any T , results in solidification. A sufficient decrease in T yields a similar effect. The solids may have several kinds of symmetry and the more complete schematic phase diagram can be found in ref. (Schultz and Kofke, 2018).

It should be noted that the separation into the two phases in the coexistence region can occur either through nucleation or by spinodal decomposition, depending on ρ and T . Both processes can be triggered by quenching from a temperature above T_c , but have a different physical mechanism. Nucleation arises as a result of a rare but large energy fluctuation and is associated with metastability (Frenkel, 1955; Feder et al., 1966; Abraham, 1975; Binder and Stauffer, 1976). On the other hand, phase separation through spinodal decomposition takes place in an initially unstable system in which all fluctuations grow because there is no energy barrier (Cahn and Hilliard, 1958; Cahn and Hilliard, 1971; Langer, 1971; Huang et al., 1974; Binder et al., 1978). Thus, the generation of metastable droplets can take place only between the binodal and spinodal lines. The spinodal line for the vdW system is also an inverted parabola that is placed within the coexistence region (cf. The bottom panel in Figure 1). The region within the spinodal line is chaotic, unstable, and beyond a

thermodynamic description. Any short-lived clusters of atoms there cannot be analogues of the “organelles.” Thus, the determination of the proper conditions for the droplet formation involves figuring out not only the position of the binodal line but also of the spinodal boundary. It should be noted that droplets of a higher (lower) density than the environment arise in the region that borders with the gas (liquid) phase. The biophysical context assumes the higher density situation.

In the absence of theoretically validated equations of state for the protein solutions, we resort to considering a simpler system: a homogeneous vdW fluid. This will allow us to test the novel concepts related to the determination of the phase diagram, giving us much-needed insight on how to deal with more complicated situations. In principle, for the vdW fluid, one can derive the free energy of the system, consistent with the equation of state, and analyze its stability. Our purpose, however, is to find alternative ways to locate the spinodal and binodal lines that could be used in molecular dynamics simulations of proteins.

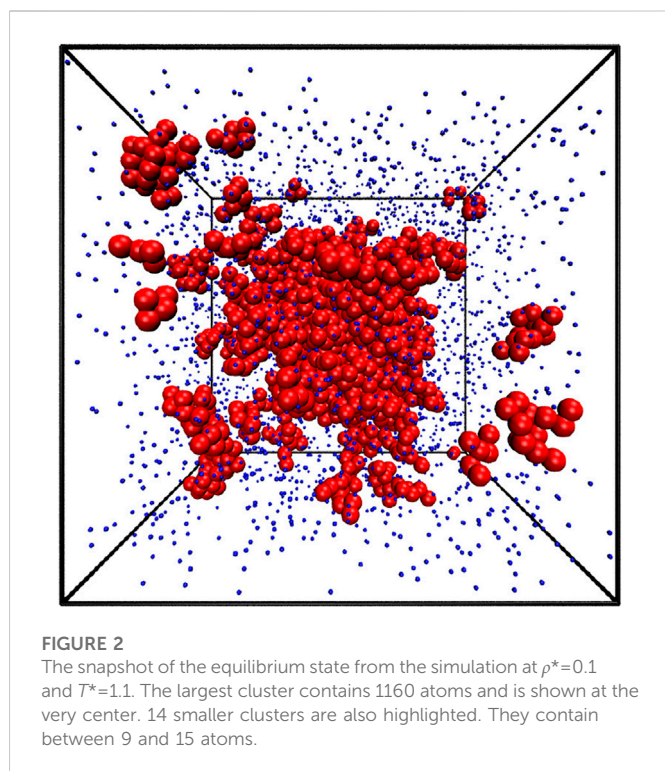
2 The phase diagram construction

A series of simulations and experimental studies (Nicolas et al., 1979; Panagiotopoulos, 1994; Baidakov et al., 2000) of the van der Waals fluids has been reviewed by Stephan et al. (Stephan et al., 2019) and the data shown in the bottom panel of Figure 1 is based on this reference. The results are presented in reduced units (the symbols are denoted by an asterisk) that involve the length parameter, σ , and the depth of the energy well, ε . Density is given in units of the number of monomers per σ^3 . For the cutoff value of 6.85σ , the critical point is at temperature T_c of 1.31 and density $\rho_c = 0.316$ that is consistent with a direct analysis of the equation of state.

The theoretical and experimental data (Stephan et al., 2019) were the references for our simulations. We performed molecular dynamics simulations for two systems of 4,000 particles: one for 4,000 non-bonded particles and the other one for 200 20-bead chains. During our simulations we monitored the cluster sizes, appearance of cavities and their volumes (Chwastyk et al., 2014a; Chwastyk et al., 2016), specific heat (Chwastyk et al., 2015; Chwastyk et al., 2017) as well as a number of other parameters to find a way to determine the phase diagram.

2.1 Details of the simulations

Our simulations were conducted by using the LAMMPS software package (Plimpton, 1995). The cut-off for LJ potential was at a distance of $r_c = 6.85\sigma$. We used the Verlet algorithm to integrate the equations of motion. The time was measured in units of $\tau_{LJ} \equiv \sqrt{m\sigma^2/\varepsilon}$, where m is the mass of each particle. This time unit corresponds to the characteristic period of undamped oscillations at the bottom of a 6–12 potential (Chwastyk et al., 2014b; Zhao et al., 2017a; Zhao et al., 2017b). We used the integration step of $\Delta t = 0.005\tau_{LJ}$ for the simulations of monomers and $\Delta t = 0.001\tau_{LJ}$ for chains. The length of our simulations was 1 000 000 and 5 000 000 steps for monomers and chains, respectively, which corresponds to 5000 τ_{LJ} of total simulation time. The trajectory analysis was done based on the last 1666 τ_{LJ} of the simulation in each case and the other part of the simulation was the equilibration. Two atoms were considered to be in contact if the distance between them does not exceed 1.3σ . Two chains



are treated as belonging to the same cluster when they have at least one inter-chain contact. As a consequence, we define a cluster as a group of beads (in the case of the simulation of monomers) or chains connected by at least one contact. The chain is defined as a line of monomers connected by harmonic potential:

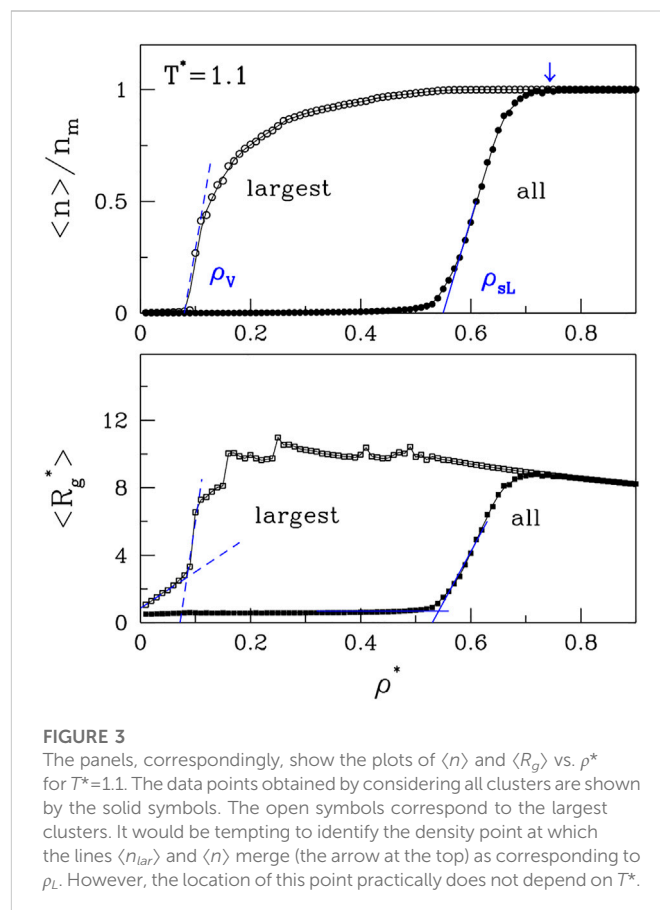
$$U_{bond}(r) = k_b(r - \sigma)^2, \quad (2)$$

where $k_b = 75000\epsilon/\sigma^2$ is a force constant, strong enough to keep two atoms at distance of σ . This assumption was established according to the results of Kevin S. Silmore *et al.* (Silmore *et al.*, 2017). We used the canonical ensemble (NVT) and the temperature was controlled by Nose-Hoover thermostat with damping parameter of $1.0\tau_{LJ}$ for monomers and $10.0\tau_{LJ}$ for chains.

2.2 The simulations results

Our simulations were conducted for 90 different densities from $\rho^* = 0.01$ to 0.90, at nine different temperatures for monomers: $T^* \in \{0.6, 0.7, 0.8, 0.9, 1.0, 1.1, 1.2, 1.25, 1.3\}$ and eight temperatures: $T^* \in \{0.5, 1.0, 1.5, 2.0, 2.5, 3.0, 3.5, 4.0\}$ for chains. The example atomic configuration is presented in Figure 2 for $\rho^* = 0.1$ and $T^* = 1.1$. The largest cluster composed of 1160 atoms is positioned in the center and 14 smaller clusters are highlighted by red larger balls. They contain from 5 to 15 atoms.

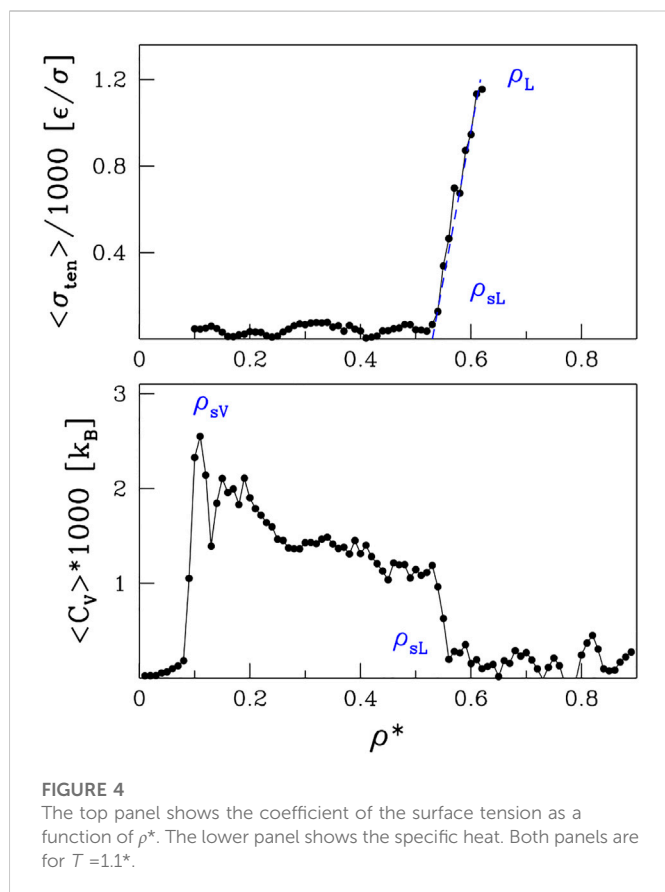
The top panels of Figure 1 pertain to our method of determination of the high-density branch, ρ_L , of the binodal line. The idea is to divide the volume into small cubes with a side of order of the size of the molecule. For polymers or proteins, the radius of gyration, r_g would be an appropriate length scale. For monatomic molecules 2σ was found to be optimal. The top left panel shows the probability distributions of the cubic bins to have 0, 1, 2, 3, etc. Atoms. At the low density ($\rho^* = 0.2$)



there is a substantial probability, P_0 , of having an empty bin. The top-right panel shows that P_0 decreases with ρ^* and at around 0.64 it approaches zero. We take this value as defining ρ_L . By considering several other temperatures we get the data points indicated as blue squares. They agree fairly well with the literature results except at the very low T^* s which appear to require longer averaging.

Let us now consider the average cluster (or droplet) sizes. These can be characterized by either the radii of gyration, R_g , or the number of molecules, n , that a droplet contains. The largest possible value of n is n_m . We find it useful to either consider averages over all clusters or only over the largest clusters. In the latter case, the corresponding average size will be denoted by n_{lar} . The results for $\langle n \rangle$ and $\langle n_{lar} \rangle$ are shown in the top panel of Figure 3. We observe that $\langle n_{lar} \rangle$ undergoes a rapid growth at the low density branch of the binodal line, ρ_v , which delineates the vapor phase. The average cluster size of all clusters also undergoes a rapid growth, but at a higher density, ρ_{sL} . The growth coincides with the upper spinodal line (the open red circles in Figure 1). The lower panel shows the corresponding plots for $\langle R_g \rangle$ and $\langle R_{g,lar} \rangle$. They basically mimic the curves related to n except that the growth of R_g for the largest cluster is affected by the fluctuating morphology of the cluster, which affects R_g while not affecting n .

In order to determine ρ_{sV} , the low density branch of the spinodal line, we study the specific heat, C_v . Since C_v is a measure of the energy fluctuations, we would expect volatile energy changes upon entering the non-thermodynamic spinodal region. Indeed, we observe sudden spikes in C_v as a function of ρ , as illustrated in the bottom panel of Figure 4 for $T^* = 1.1$. The tallest of them is on the low-density side and its location is marked by open red circles on the left side of Figure 1.

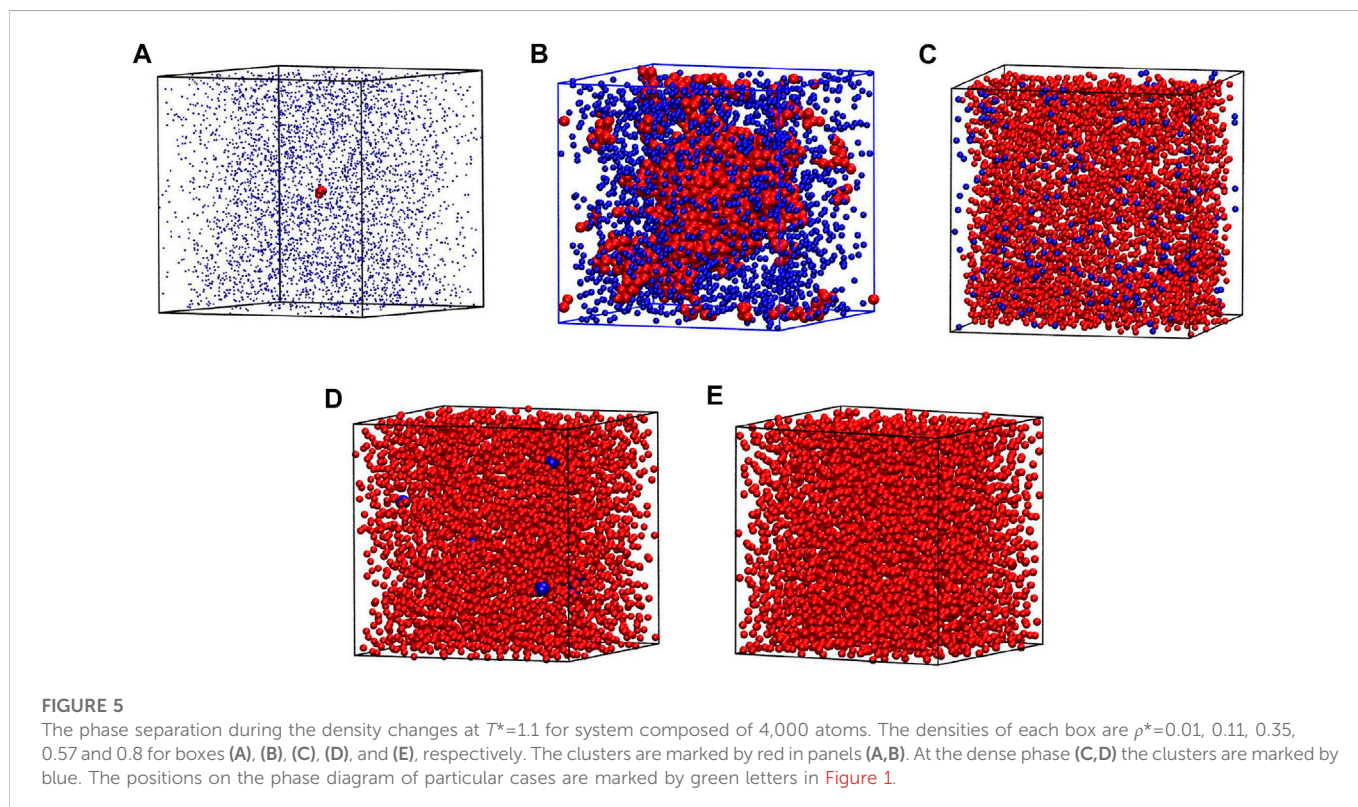


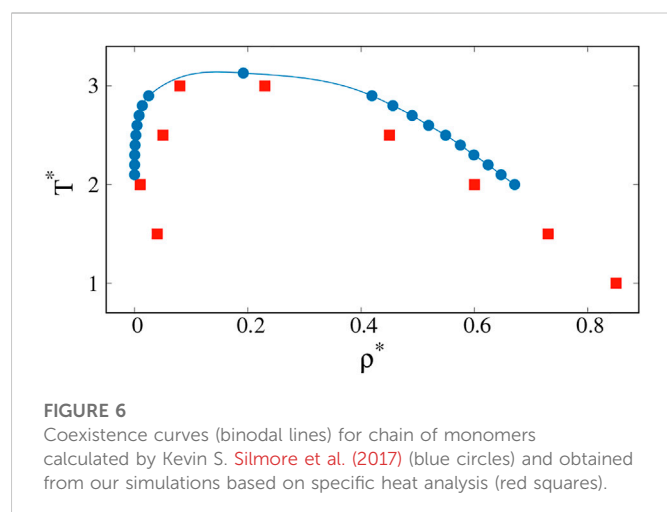
When going to higher densities, there is a sudden drop in C_V that coincides with ρ_{sL} obtained from $\langle n \rangle$.

Yet another way to assess the boundary of the spinodal region is through the surface tension, σ_{ten} . It can be derived, both theoretically and experimentally, by invoking the energy equipartition theorem (Caragine et al., 2018; Caragine and Haley, 2019) leading to $\sigma_{ten} = k_B T / u^2$ where u^2 is the fluctuation in the droplet linear size and k_B is the Boltzmann constant. In molecular dynamics, we take u^2 to be a fluctuation of R_g and average it over time. We perform this procedure for sufficiently large droplets, as they are better defined. However, to avoid the finite-size effects, we do not consider droplets that span the whole system. The surface tension, σ_{ten} , calculated in this manner is shown in the upper panel of Figure 4 for $T^* = 1.1$. The behavior of σ_{ten} as a function of density is rather irregular in the spinodal region but then a nearly monotonic increase is observed between ρ_{sL} and ρ_L . The phase separation induced by the density changes at $T^* = 1.1$ is presented schematically in Figure 5. The nucleation process can be observed in panels B and D for light and dense phases, respectively. Panels A and E represent one-phase regimes.

3 The phase diagram for chains of monomers

Proteins differ from the Lennard-Jones atoms discussed so far in two major ways: first, their molecules are in the form of chains, and second, the monomers in the chains are of a heterogeneous nature as





they represent 20 types of amino acid. The second aspect requires special studies along the lines of Dignon et al. (Dignon et al., 2018a; Dignon et al., 2018b; Dignon et al., 2019) or Mioduszeowski et al. (Mioduszeowski and Cieplak, 2018; Mioduszeowski and Cieplak, 2020; Mioduszeowski and Cieplak, 2021) who use different coarse-grained models to analyze the protein dynamics. In addition, proteins may have inverted binodal lines when hydrophobic effects intervene (Li et al., 2002; Urry et al., 2002; Dignon et al., 2019). We now consider the first of these aspects by performing molecular dynamics simulations for $n_m = 400$ chain molecules of length 20 each. The atoms in the chains are connected at a distance of σ . The binodal lines for this system have been derived by Silmore et al. (Silmore et al., 2017) by using the procedure of Rowlinson and Widom (Rowlinson and Widom, 1982) in which one starts with a dense blob of molecules in the center of an elongated periodic box and reaches a heterogeneous equilibrium. These results are presented by blue points in Figure 6. The chains exhibit more cohesion, and therefore the critical point is moved up in temperature in comparison to the monomeric system.

The clusters that are analogues of the biological droplets are those that should be present immediately to the left of the left branch of the spinodal line, i.e. close to the gas phase. To the right of the right branch of the spinodal line, there are droplets of the low density regions that are essentially like cavities in the liquid phase. The cavities disappear on crossing the binodal line towards the single-component liquid phase. In numerical practice, finding the left branch of the spinodal line can be achieved by considering C_v . This works also for the right-hand side spinodal line but monitoring the surface tension offers an additional tool. Our results for the determination of the spinodal line, based on the C_v analysis are presented by red squares in Figure 6.

4 Conclusion

In principle, a precise determination of both the binodal and spinodal line requires procedures of finite-size scaling. Our purpose here, however, was to determine quantities to accomplish the task

of determining the region in which the metastable droplets could be studied theoretically. In previous theoretical studies (Dignon et al., 2018a; Dignon et al., 2018b; Mioduszeowski and Cieplak, 2018; Dignon et al., 2019; Mioduszeowski and Cieplak, 2020) analyzing proteinaceous droplets, no attempt was made to locate spinodal lines within the two-phase region. The proposed approach should help in such cases, as it allows for the determination of binodal and spinodal line positions for fluids of complex composition.

Data availability statement

The original contributions presented in the study are included in the article/Supplementary Material, further inquiries can be directed to the corresponding author.

Author contributions

All of the authors developed the model, analysed results and wrote the paper. PQ performed the simulations. The manuscript was submitted after the death of MC.

Funding

This research has received support from the National Science Centre (NCN), Poland, under grant No. 2018/31/B/NZ1/00047 and the European H2020 FETOPEN-RIA-2019-01 grant PathoGelTrap No. 899616. The computer resources were supported by the PL-GRID infrastructure. This project is also a part of the European COST Action EUTOPIA.

Acknowledgments

Discussions with P. R. F. de Carvalho and his technical help are appreciated. We are grateful for comments of Piotr Szymczak about the manuscript.

Conflict of interest

The authors declare that the research was conducted in the absence of any commercial or financial relationships that could be construed as a potential conflict of interest.

Publisher's note

All claims expressed in this article are solely those of the authors and do not necessarily represent those of their affiliated organizations, or those of the publisher, the editors and the reviewers. Any product that may be evaluated in this article, or claim that may be made by its manufacturer, is not guaranteed or endorsed by the publisher.

References

- Abraham, F. F. (1975). *Homogeneous nucleation theory*. New York: Academic Press.
- Babu, M. M., van der Lee, R., de Groot, N. S., and Gsponer, J. (2011). Intrinsically disordered proteins: Regulation and disease. *Curr. Opin. Struct. Biol.* 21, 432–440. doi:10.1016/j.sbi.2011.03.011
- Baidakov, V. G., Chernykh, G. G., and Protchenko, S. P. (2000). Effect of the cut-off radius of the intermolecular potential on phase equilibrium and surface tension in Lennard-Jones systems. *Chem. Phys. Lett.* 321, 315–320. doi:10.1016/s0009-2614(00)00217-7
- Banani, S. F., Lee, H. O., Hyman, A. A., and Rosen, M. K. (2017). Biomolecular condensates: Organizers of cellular biochemistry. *Nat. Rev. Mol. Cell Biol.* 18, 285–298. doi:10.1038/nrm.2017.7
- Binder, K., Billotet, C., and Mirol, P. (1978). On the theory of spinodal decomposition in solid and liquid binary mixtures. *Z. Phys. B* 30, 183–195. doi:10.1007/bf01320985
- Binder, K., and Stauffer, D. (1976). Statistical theory of nucleation, condensation and coagulation. *Adv. Phys.* 25, 343–396. doi:10.1080/00018737600101402
- Boeynaems, S., Alberti, S., Fawzi, N. L., Mittag, T., Polymenidou, M., Rousseau, F., et al. (2018). Protein phase separation: A new phase in cell biology. *Trends Cell Biol.* 28, 420–435. doi:10.1016/j.tcb.2018.02.004
- Brangwynne, C. P., Mitchison, T. J., and Hyman, A. A. (2011). Active liquid-like behavior of nucleoli determines their size and shape in *Xenopus laevis* oocytes. *Proc. Natl. Acad. Sci. U. S. A.* 108, 4334–4339. doi:10.1073/pnas.1017150108
- Brangwynne, C. P., Eckmann, C. R., Courson, D. S., Rybarska, A., Hoege, C., Gharakhani, J., et al. (2009). Germline P granules are liquid droplets that localize by controlled dissolution/condensation. *Science* 324, 1729–1732. doi:10.1126/science.1172046
- Cahn, J. W., and Hilliard, J. E. (1958). Free energy of a nonuniform system. I. Interfacial free energy. *J. Chem. Phys.* 28, 258–267. doi:10.1063/1.1744102
- Cahn, J. W., and Hilliard, J. E. (1971). Spinodal decomposition: A reprise. *Acta Met.* 19, 151–161. doi:10.1016/0001-6160(71)90127-1
- Caragine, C. M., and Haley, S. C. (2019). Nucleolar dynamics and interactions with nucleoplasm in living cells. *eLife* 8, e47533. doi:10.7554/eLife.47533
- Caragine, C. M., Haley, S. C., and Zidovska, A. (2018). Surface fluctuations and coalescence of nucleolar droplets in the human cell nucleus. *Phys. Rev. Lett.* 121, 148101. doi:10.1103/physrevlett.121.148101
- Chwastyk, M., and Cieplak, M. (2020). Conformational biases of α -synuclein and formation of transient knots. *J. Phys. Chem. B* 124, 11–19. doi:10.1021/acs.jpcc.9b08481
- Chwastyk, M., Galera-Prat, A., Sikora, M., Gómez-Sicilia, Á., Carrión-Vázquez, M., and Cieplak, M. (2014). Theoretical tests of the mechanical protection strategy in protein nanomechanics. *Proteins* 82, 717–726. doi:10.1002/prot.24436
- Chwastyk, M., Jaskolski, M., and Cieplak, M. (2014). Structure-based analysis of thermodynamic and mechanical properties of cavity-containing proteins – case study of plant pathogenesis-related proteins of class 10. *FEBS J.* 281, 416–429. doi:10.1111/febs.12611
- Chwastyk, M., Jaskolski, M., and Cieplak, M. (2016). The volume of cavities in proteins and virus capsids. *Proteins* 84, 1275–1286. doi:10.1002/prot.25076
- Chwastyk, M., Poma Bernaola, A., and Cieplak, M. (2015). Statistical radii associated with amino acids to determine the contact map: Fixing the structure of a type I cohesin domain in the Clostridium thermocellum cellulosome. *Phys. Biol.* 12, 046002. doi:10.1088/1478-3975/12/4/046002
- Chwastyk, M., Vera, A. M., Galera-Prat, A., Gunnoo, M., Thompson, D., Carrión-Vázquez, M., et al. (2017). Non-local effects of point mutations on the stability of a protein module. *J. Chem. Phys.* 147, 105101. doi:10.1063/1.4999703
- de Aquino, B. R. H., Chwastyk, M., Mioduszecki, L., and Cieplak, M. (2020). Networks of interbasin traffic in intrinsically disordered proteins. *Phys. Rev. Res.* 2, 013242. doi:10.1103/physrevresearch.2.013242
- Dignon, G. L., Zheng, W., Best, R. B., Kim, Y. C., and Mittal, J. (2018). Relation between single-molecule properties and phase behavior of intrinsically disordered proteins. *Proc. Natl. Acad. Sci. U. S. A.* 115, 9929–9934. doi:10.1073/pnas.1804177115
- Dignon, G. L., Zheng, W., Kim, Y. C., Best, R. B., and Mittal, J. (2018). Sequence determinants of protein phase behavior from a coarse-grained model. *PLoS Comput. Biol.* 14, e1005941. doi:10.1371/journal.pcbi.1005941
- Dignon, G. L., Zheng, W., Kim, Y. C., and Mittal, J. (2019). Temperature-controlled liquid-liquid phase separation of disordered proteins. *ACS Cent. Sci.* 5, 821–830. doi:10.1021/acscentsci.9b00102
- Dunker, A. K., Silman, I., Uversky, V. N., and Sussman, V. L. (2008). Function and structure of inherently disordered proteins. *Curr. Opin. Struct. Biol.* 18, 756–764. doi:10.1016/j.sbi.2008.10.002
- Dyson, H. J., and Wright, P. E. (2005). Intrinsically unstructured proteins and their functions. *Nat. Rev. Mol. Cell Biol.* 6, 197–208. doi:10.1038/nrm1589
- Elbaum-Garfinkle, S. (2019). Matter over mind: Liquid phase separation and neurodegeneration. *JBC Rev.* 294, 7160–7168. doi:10.1074/jbc.rev118.001188
- Feder, J., Russell, K. C., Lothe, J., and Pound, G. M. (1966). Homogeneous nucleation and growth of droplets in vapours. *Adv. Phys.* 15, 111–178. doi:10.1080/00018736600101264
- Ferreon, A. C. M., Moran, C. R., Gambin, Y., and Deniz, A. A. (2010). Single-molecule fluorescence studies of intrinsically disordered proteins. *Methods Enzymol.* 472, 179–204. doi:10.1016/S0076-6879(10)72010-3
- Fink, A. L. (2005). Natively unfolded proteins. *Curr. Opin. Struct. Biol.* 15, 35–41. doi:10.1016/j.sbi.2005.01.002
- Frenkel, J. (1955). *Kinetic theory of nucleation*. New York: Dover.
- Hensen, J. P., and McDonald, I. R. (1973). *Theory of simple liquids*. New York: Academic Press.
- Huang, J. S., Goldburg, W. I., and Bjerkaas, A. W. (1974). Study of phase separation in a critical binary liquid mixture: Spinodal decomposition. *Phys. Rev. Lett.* 32, 921–923. doi:10.1103/physrevlett.32.921
- Langer, J. S. (1971). Theory of spinodal decomposition in alloys. *Ann. Phys.* 65, 53–86. doi:10.1016/0003-4916(71)90162-x
- Li, B., Alonso, D. O. V., and Daggett, V. (2002). Stabilization of globular proteins via introduction of temperature-activated elastin-based switches. *Structure* 10, 989–998. doi:10.1016/s0969-2126(02)00792-x
- Mioduszecki, L., and Cieplak, M. (2018). Disordered peptide chains in an α -C-based coarse-grained model. *Phys. Chem. Chem. Phys.* 20, 19057–19070. doi:10.1039/c8cp03309a
- Mioduszecki, L., and Cieplak, M. (2020). Protein droplets in systems of disordered homeopeptides and the amyloid glass phase. *Phys. Chem. Chem. Phys.* 22, 15592–15599. doi:10.1039/d0cp01635g
- Mioduszecki, L., and Cieplak, M. (2021). Viscoelastic properties of wheat gluten in a molecular dynamics study. *PLoS Comput. Biol.* 17, e1008840. (in press). doi:10.1371/journal.pcbi.1008840
- Nicolas, J. J., Gubbins, K. E., Street, B., and Tildesley, D. J. (1979). Equation of state for the Lennard-Jones fluid. *Mol. Phys.* 37, 1429–1454. doi:10.1080/00268977900101051
- Panagiotopoulos, A. Z. (1994). Molecular simulation of phase coexistence: Finite-size effects and determination of critical parameters for two- and three-dimensional Lennard-Jones fluids. *Int. J. Thermophys.* 15, 1057–1072. doi:10.1007/bf01458815
- Plimpton, S. (1995). Fast parallel algorithms for short-range molecular dynamics. *J. Comp. Phys.* 117, 1–19. doi:10.1006/jcph.1995.1039
- Rowlinson, J. S., and Widom, B. (1982). *Molecular theory of capillarity*. Oxford: Clarendon Press.
- Schultz, A. J., and Kofke, D. A. (2018). Comprehensive high-precision high-accuracy equation of state and coexistence properties for classical Lennard-Jones crystals and low-temperature fluid phases. *J. Chem. Phys.* 149, 204508. doi:10.1063/1.5053714
- Shin, Y., and Brangwynne, C. P. (2017). Liquid phase condensation in cell physiology and disease. *Science* 357, eaaf4382. doi:10.1126/science.aaf4382
- Silmore, K. S., Howard, M. P., and Panagiotopoulos, A. Z. (2017). Vapour-liquid phase equilibrium and surface tension of fully flexible Lennard-Jones chains. *Molec. Phys.* 115, 320–327. doi:10.1080/00268976.2016.1262075
- Stephan, S., Thol, M., Vrabec, J., and Hasse, H. (2019). Thermophysical properties of the Lennard-Jones fluid: Database and data assessment. *J. Chem. Info. Model.* 59, 4248–4265. doi:10.1021/acs.jcim.9b00620
- Urry, D. W., Hugel, T., Seitz, M., Gaub, H. E., Scheiba, L., Dea, J., et al. (2002). Elastin: A representative ideal protein elastomer. *Phil. Trans. R. Soc. Lond. B* 357, 169–184. doi:10.1098/rstb.2001.1023
- Uversky, V. N., and Dunker, A. K. (2010). Understanding protein non-folding. *Biochem. Biophys. Acta* 1804, 1231–1264. doi:10.1016/j.bbapap.2010.01.017
- Uversky, V. N. (2002). Natively unfolded proteins: A point where biology waits for physics. *Prot. Sci.* 11, 739–756. doi:10.1110/ps.4210102
- Wright, P. E., and Dyson, H. J. (2015). Intrinsically disordered proteins in cellular signalling and regulation. *Nat. Rev. Mol. Cell Biol.* 6, 18–29. doi:10.1038/nrm3920
- Zhao, Y., Chwastyk, M., and Cieplak, M. (2017). Structural entanglements in protein complexes. *J. Chem. Phys.* 146, 225102. doi:10.1063/1.4985221
- Zhao, Y., Chwastyk, M., and Cieplak, M. (2017). Topological transformations in proteins: Effects of heating and proximity of an interface. *Sci. Rep.* 7, 39851. doi:10.1038/srep39851